Ellipsometry on Sputter Deposited Tin Oxide Films: Optical Constants vs. Stoichiometry, Hydrogen content, and Amount of Electrochemically Intercalated Lithium

J. Isidorsson and C. G. Granqvist

Department of Materials Science, The Ångström Laboratory, Uppsala University,

P O Box 534, S-751 21 Uppsala, Sweden

K. von Rottkay and M. Rubin

Lawrence Berkeley National Laboratory, University of California, Berkeley,

CA 94720, USA

ABSTRACT

Tin oxide thin films were deposited by reactive radio frequency magnetron sputtering onto In_2O_3:Sn coated and bare glass substrates. Optical constants in the 300-2500 nm wavelength range were determined by a combination of variable angle spectroscopic ellipsometry and spectrophotometric transmittance measurements. Surface roughness was modeled from optical measurements and compared with atomic force microscopy. The two techniques gave consistent results. The fit between experimental optical data and model results could be significantly improved by assuming that the refractive index of the Sn oxide varied across the film thickness. By varying the oxygen partial pressure during deposition, it was possible to obtain films whose

complex refractive index changed at the transition from SnO to SnO_2. An addition of hydrogen gas during sputtering led to lower optical constants in the full spectral range in connection with a blue shift of the band gap. Electrochemical intercalation of lithium ions into the Sn oxide films raised their refractive index and enhanced their refractive index gradient.

Keywords: Tin oxide, thin films, sputtering, optical constants, refractive index, ellipsometry, atomic force microscopy.

I. INTRODUCTION

This paper regards the optical properties of Sn-oxide-based films prepared so that their contents of oxygen, hydrogen, and lithium lie within wide ranges. The optical properties are studied by ellipsometry. Sn-oxide-based films have diverse applications in optical technology. The most commonly used films are well-crystallized SnO_2 layers doped with Sb, F, or oxygen vacancies; they can serve as transparent electrical conductors [1], low-emittance coatings [1], and frost-preventing surfaces [2]. These applications rely on free electrons originating from the ionization of dopants. Our present work concerns Sn-based materials mainly for use in solid state opto-ionics, such as in non-coloring counter electrodes for electrochromic smart windows [3]. These applications hinge on the ability of the considered material to sustain mixed conduction of ions and electrons [3]. We also note that Sn oxide is of interest for gas sensors [4,5], and that it has recently been suggested as a novel material for innovative battery technology [6,7,8].

Electrochromic Sn oxide films have been prepared by dip coating [9,10,11] and magnetron sputtering [12], and a change in the valence state of the tin atoms due to electrochemical Li^+ ion intercalation has been reported [13]. Sn oxide has the interesting property of being able to serve both as transparent conductor and non-coloring Li^+ ion conducting electrode, thereby giving the possibility to simplify the production of electrochromic devices.

For a deeper understanding of electrochromic Sn oxide it is necessary to examine its optical properties in detail. The optical indices of Sn oxide thin films for transparent electrical conductors and low-emittance coatings have been investigated in

the past [14-20]; usually a crystalline structure is desirable for these applications. Disordered Sn oxide is able to achieve a larger Li^+ intercalation than crystalline Sn oxide and is therefore more suitable for applications in solid state ionics [12]. The present investigation considers the optical constants of "amorphous" Sn oxide, especially the roles of varying stoichiometry, hydrogen incorporation, and electrochemically introduced lithium ions.

In section II we describe the sputtering process and report experimental data from resistivity measurements, Rutherford backscattering spectrometry (RBS), and atomic force microscopy (AFM). Electrochemical intercalation of lithium into the Sn oxide lattice is discussed, and nuclear reaction analysis (NRA) data on the lithium distribution in the films are presented. Section III presents ellipsometric and spectrophotometric results and describes the optical models used in our calculations. Effects on the optical data of varying oxygen content during the deposition process, of addition of hydrogen in the sputter gas, and of electrochemical intercalation of lithium into the Sn oxide film are reported in detail. The optical modeling employs a two-film configuration comprising a transparent and electrically conducting base layer of In_2O_3:Sn (i.e., ITO) and a Sn oxide top layer. Section IV then discusses the results and elaborates on the effect of the sputter gas composition on the optical constants. We also investigate the influence of Li^+ intercalation on the optical constants and present evidence for an increasing gradient of the optical constants over the film cross-section after lithiation. A brief discussion and concluding remarks are given in Sec. V.

II. FILM PREPARATION AND CHARACTERIZATION

The films were deposited by reactive rf magnetron sputtering in a Balzers UTT 400 turbo molecular pumped vacuum deposition unit equipped with several US gun magnetron cathodes. A base pressure of 10^{-7} Torr was assured by regular baking of the vacuum unit during 10 h periods. A 5-cm-diameter tin target of 99.999% purity was used together with sputter gases of 99.998% purity. Tin oxide films were deposited at a pressure of 30 mTorr with a rf power of 200 W in an Ar/O_2 gas mixture ranging from 59/1 to 51/9 as well as in an $Ar/O_2/H_2$ mixture ranging from 51/9/2 to 51/9/10. Pertinent partial pressures for oxygen and hydrogen are denoted $p(O_2)$ and $p(H_2)$, respectively. The distance between target and substrate was about 13 cm. Films for optical and electrochemical investigation where grown on unheated 1 mm thick glass slides with and without transparent and conducting ITO layers having a resistance of 15 Ω/square.

Film thickness *d*, measured by surface profilometry employing a Tencor Alpha Step instrument, lay between 144 and 478 nm. These values were subsequently refined by ellipsometry. The growth rate *r* was between 11 and 23 nm/min. Figure 1a shows *r* as a function of $p(O_2)$. The highest growth rate occurs for $p(O_2) \sim 1$ mTorr.

The mass density δ of the Sn oxide films was determined by RBS using 1.95 MeV alpha particles in back scattering geometry. Figure 1b illustrate δ versus $p(O_2)$. The lowest density coincides with the highest deposition rate. Figure 1c combines the previous results to show the mass deposition rate. It is interesting to note that there is little variation of the mass deposition rate at low oxygen partial pressures, while the film growth rate in Fig. 1a varies considerably.

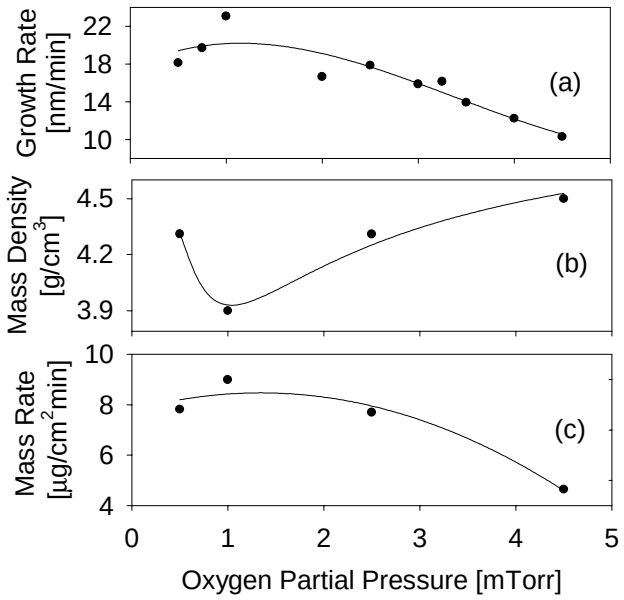

Figure 1. Growth rate (part a), mass density (part b), and product of these two entities (part c) vs. oxygen partial pressure for sputter deposited Sn oxide films. Symbols denote experimental data and curves were drawn for convenience.

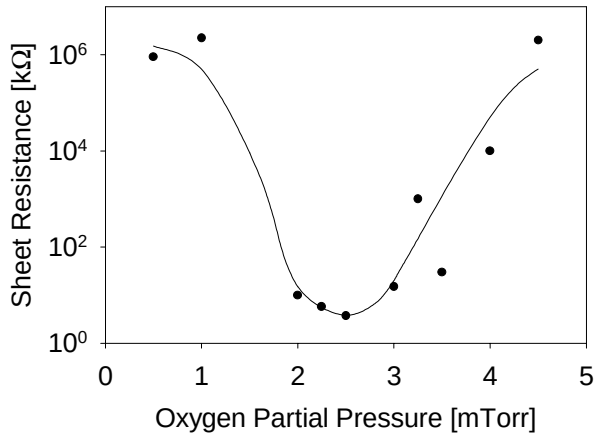

Figure 2. Sheet resistance vs. oxygen partial pressure for sputter deposited Sn oxide films. Symbols denote experimental data and and curves were drawn for convenience.

Electrical properties contain important information on the structure and stoichiometry of Sn oxide films [1,12]. We measured the sheet resistance R_{sq} by pressing a probe with two rows of spring-loaded pin contacts against the film surface. From Fig. 2 it is evident that R_{sq} has a pronounced minimum at a specific oxygen partial pressure. For $p(O_2)$ < 2 mTorr, the specimen is SnO-rich and has a brownish appearance. At $p(O_2)$ ~ 2 mTorr, the structure is SnO_2-like and has oxygen vacancies serving as *n*-type donors; these films are transparent. At higher oxygen partial pressures, finally, the stoichiometry approaches SnO_2. The results in Fig. 2 are in good agreement with earlier ones [12].

Surface reliefs of as-deposited Sn oxide films were obtained by AFM using a NanoScope III instrument with an etched silicon cantilever having a tip radius of 10 nm and 35° apex angle. Data were taken in ambient air with a contact force of about 10^{-7} N. Scans were made over areas from 50 x 50 μm to 1 x 1 μm with a resolution of 256 x 256 pixels. Figure 3 illustrates a typical AFM image. Rounded protrusions with a lateral extent of 20 to 100 nm are apparent. Values of RMS and peak-to-peak roughness are presented in Fig. 4 as obtained from analyses of several different 1×1 μm images of each sample. Both roughness measures increase linearly with increasing magnitude of $p(O_2)$. The peak-to-peak value is larger than the RMS quantity by roughly an order of magnitude. Figure 4 also shows the "optical roughness" as modeled from ellipsometry data to be discussed below. Its variation as a function of $p(O_2)$ agrees well with the peak-to-peak value from AFM, but the numerical values are offset. A more detailed discussion will follow in Sec. III A.

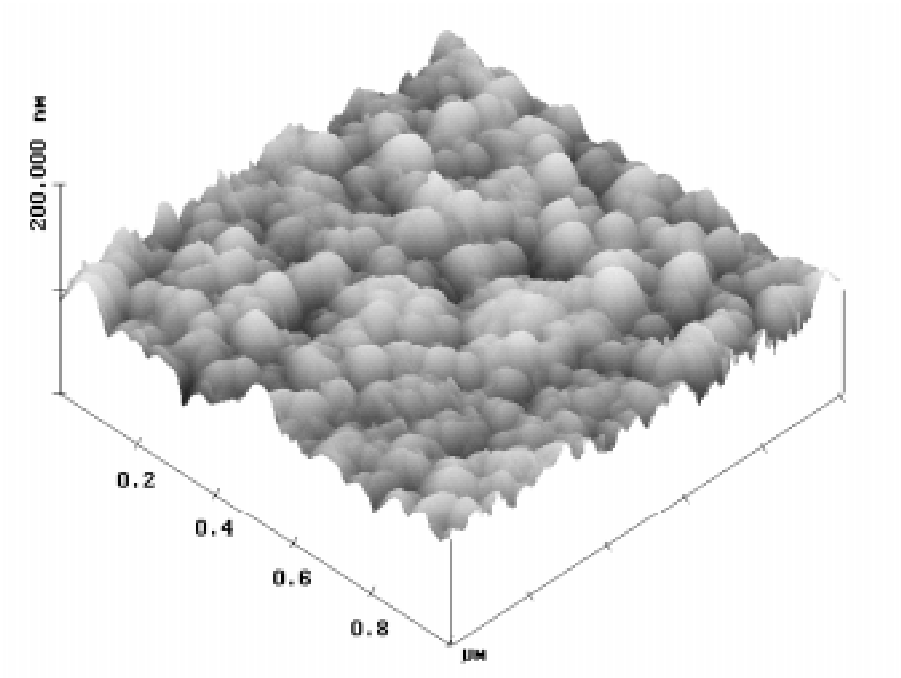

Figure 3. Atomic force micrograph of the surface of a Sn oxide film sputter deposited at an oxygen partial pressure of 4.5 mTorr.

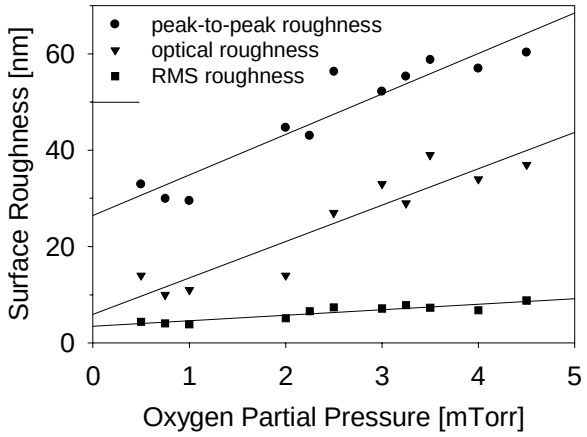

Figure 4 Root-mean-square (RMS) roughness, peak-to-peak roughness, and "optical roughness" vs. oxygen partial pressure for sputter deposited Sn oxide films. The former two sets of data were recorded by atomic force microscopy (AFM). Symbols denote experimental data and lines were drawn for convenience.

Electrochemical Li^+ ion intercalation was performed in a glove box with a helium atmosphere containing less than 1 ppm H_2O, using an Arbin potentiostat. The electrolyte was 1M $LiClO_4$ in propylene carbonate. Lithiation was accomplished by applying a constant current of 10 μA to an electrode with an area of about 3 cm^2. The potential was varied from the open circuit value to a predetermined potential being 2.0, 1.7, or 1.5 V vs. Li/Li^+. When this latter potential was reached, conditions were kept constant overnight. The samples were subsequently cleaned with tetrahydrofuran and were allowed to dry in the glove box atmosphere for 30 minutes. Ellipsometric data and spectrophotometric transmission spectra were recorded immediately after the sample was taken out of the He atmosphere.

The lithium distribution in the Sn oxide film was investigated by NRA via the reaction 1.5 MeV $^7Li(p, \alpha)^4He$. Figure 5 shows the intensity of the lithium signal in counts as a function of channel number. High channel numbers pertain to the surface region of the Sn-oxide-based film and low channel numbers to the inner interface towards the ITO base layer. It is clear that the concentration of lithium is highest at the surface and decreases almost linearly with distance from the surface in the sample intercalated to 1.7 V vs. Li/Li^+. When intercalation was performed to 1.5 V vs. Li/Li^+, the Li concentration appears to have reached a state of saturation in the outer half of the film, while the concentration then decreases rather linearly and reaches zero at the ITO base.

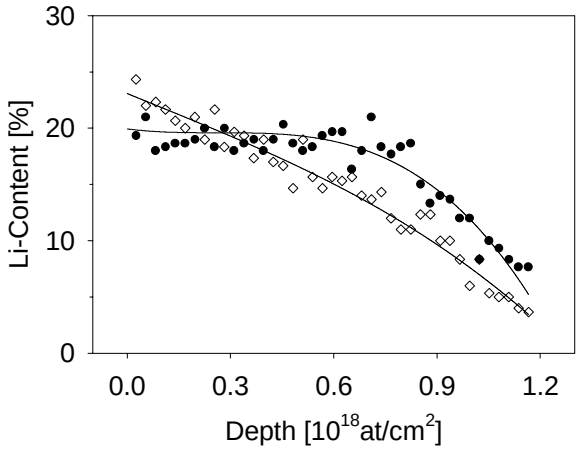

Figure 5. Lithium content vs. atomic depth from the surface for electrochemically lithiated Sn oxide films. The data was obtained from nuclear reaction analysis. Open symbols denote SnO_2 lithiated to 1.7V vs. Li and solid symbols to 1.5V vs. Li. Curves were drawn for convenience.

III. OPTICAL PROPERTIES: MEASUREMENTS AND EVALUATIONS

A. General

Optical measurements were made in the wavelength interval $280 < \lambda < 1700$ nm with a J.A. Woollam Co. variable-angle spectroscopic ellipsometer using a rotating analyzer. The instrument records the ratio of the complex Fresnel reflection coefficients $\tilde{r}$ for *s* and *p* polarization in terms of the ellipsometric parameters Ψ and Δ according to

$$\frac{\tilde{r}_p}{\tilde{r}_s} = \tan(\Psi)\cdot\exp(i\Delta)\,. \qquad (1)$$

Ellipsometric measurements were taken at 3 to 5 specific angles in the range $56° < \Theta < 75°$ to obtain adequate sensitivity over the full spectral interval. Standard deviations of ellipsometric measurements could be determined experimentally by recording each

data point as the average of 30 revolutions of the analyzer. Spectrophotometric transmittance *T* measurements in the range $250 < \lambda < 2500$ nm were routinely added. These latter data were taken at normal incidence using a Perkin-Elmer Lambda 19 spectrophotometer. The standard deviation of the transmittance measurements was assessed by comparing multiple measurements; it was estimated to be 0.1% for $250 < \lambda < 860$ nm and 0.2% for $860 < \lambda < 2500$ nm. Optical measurements were made separately on the ITO coated substrate. No optical anisotropy was anticipated or modeled because Sn oxide films sputtered at 30 mTorr are amorphous as judged by X-ray diffraction [12].

A parametric semiconductor model [21,22] was used to represent the dispersion in the optical properties for the Sn oxide films. This model corresponds to the superposition of many Lorentzian oscillators of slightly different energies. Employing this model, we obtained a very good fit to experimental data also in the case of the model parameters being reduced to give a simpler Gaussian form representing strongly inhomogeneous broadening. Even a single Lorentz oscillator model was capable of giving a good fit over most of the spectrum. The main improvement using the Gaussian model rather than the single Lorentz oscillator was found in the region just above the band gap for Sn oxide, where a Gaussian broadening of the oscillator describes the relatively abrupt absorption edge better than the homogeneous Lorentzian broadening [23].

Ellipsometric and spectrophotometric data were fitted together by weighting both types of data according to their standard deviations. The numerical iteration was performed utilizing a Levenberg-Marquardt algorithm until a global minimum was reached for the biased mean square error (MSE), defined by [24],

$$\mathrm{MSE} = \frac{1}{N - M} \sum_{\lambda} \left\{ \sum_{\Theta} \left[\left(\frac{\Psi_{\lambda,\Theta,\mathrm{cal}} - \Psi_{\lambda,\Theta,\mathrm{exp}}}{\sigma_{\lambda,\Theta,\Psi}} \right)^2 + \left(\frac{\Delta_{\lambda,\Theta,\mathrm{cal}} - \Delta_{\lambda,\Theta,\mathrm{exp}}}{\sigma_{\lambda,\Theta,\Delta}} \right)^2 \right] + \left(\frac{T_{\lambda,\mathrm{cal}} - T_{\lambda,\mathrm{exp}}}{\sigma_T} \right)^2 \right\}. \quad (2)$$

Here N is the total number of experimental observations, M is the number of fitting parameters, σ is the standard deviation, and the indices λ and Θ denote data points taken at different wavelengths and angles. The subscripts “cal” and “exp” refer to calculated and experimental values, respectively. It is necessary to include backside reflection into the model for a semitransparent film if the glass substrate is not roughened or reflections from the backside are avoided by some other method. We roughened the back surface of the samples by means of sandblasting, except for those samples intended for electrochemical treatment for which transmittance measurements were recorded both before and after the electrochemical lithiation.

B. Structural models for the samples

The analysis of optical data requires a structural model of the sample. In the simplest case, this consists of a single homogeneous layer for both substrate and thin film. However, in our case the Sn oxide films were deposited onto ITO coated glass so that at least one additional layer is necessary. The ITO, which in itself is a very demanding material to properly measure and analyze [25], had to be taken to exhibit an index gradient between the portion close to the substrate and that close to the surface [26,27].

Interface and surface roughness influence the optical properties of a sample and can be optically represented, at least to a first approximation, by an effective medium [28,29,30]. At an interface one would choose a layer of an effective medium constructed from the dielectric properties of the two materials at either side of the

boundary. The thickness of the effective medium layer then corresponds to the extent of the interface transition region. A mixture of a solid material with voids can sometimes represent surface roughness [31]. Lacking detailed microstructural information, we used the Bruggeman effective medium theory [32]. Any theory of this kind requires that the material be adequately describable by an effective dielectric constant over a region much smaller than the wavelength of the incident light.

The optically determined thickness of the roughness layer was compared with AFM data. Figure 4 depicted the thickness of the roughness layer, as evaluated from AFM using two techniques, to those extracted from the optical measurements. The AFM thickness that is in best accordance with the one determined optically corresponds to the difference between the highest and the lowest point on the image. The resolution of the AFM allows us to measure features smaller than the wavelength of the light used in the optical investigation, and thus AFM may be expected to yield a thicker roughness layer.

Both AFM and ellipsometry show that the samples deposited at low oxygen partial pressure are smoother than those deposited at high oxygen partial pressure, and that there is a linear relationship between roughness and $p(O_2)$. In the specific case, the AFM roughness appears to be offset by about 20 nm from results of the optical model.

For Sn oxide films deposited at $p(O_2) > 1.5$, the surface roughness model did not result in satisfying fits to experimental data, and it was necessary to include a void grading in the Sn oxide layer itself thereby simulating a less dense surface region. Fits to a graded 5-layer model for Sn oxide films sputter deposited at $p(O_2) = 4.5$ mTorr onto ITO yielded typically MSE = 19, whereas MSE = 33 was found for the model with a homogenous layer plus surface roughness. Figure 6 shows the excellent

agreement between experimental and calculated data for Ψ, Δ and *T* that can be accomplished in the case of a graded layer model. In order to eliminate spurious combinations of fitting parameters for such a complicated model, Sn oxide films were also deposited onto glass substrates without the ITO layer. Optical measurements on those films showed the same index gradient as the films on ITO-coated glass, which lends credence to our analysis.

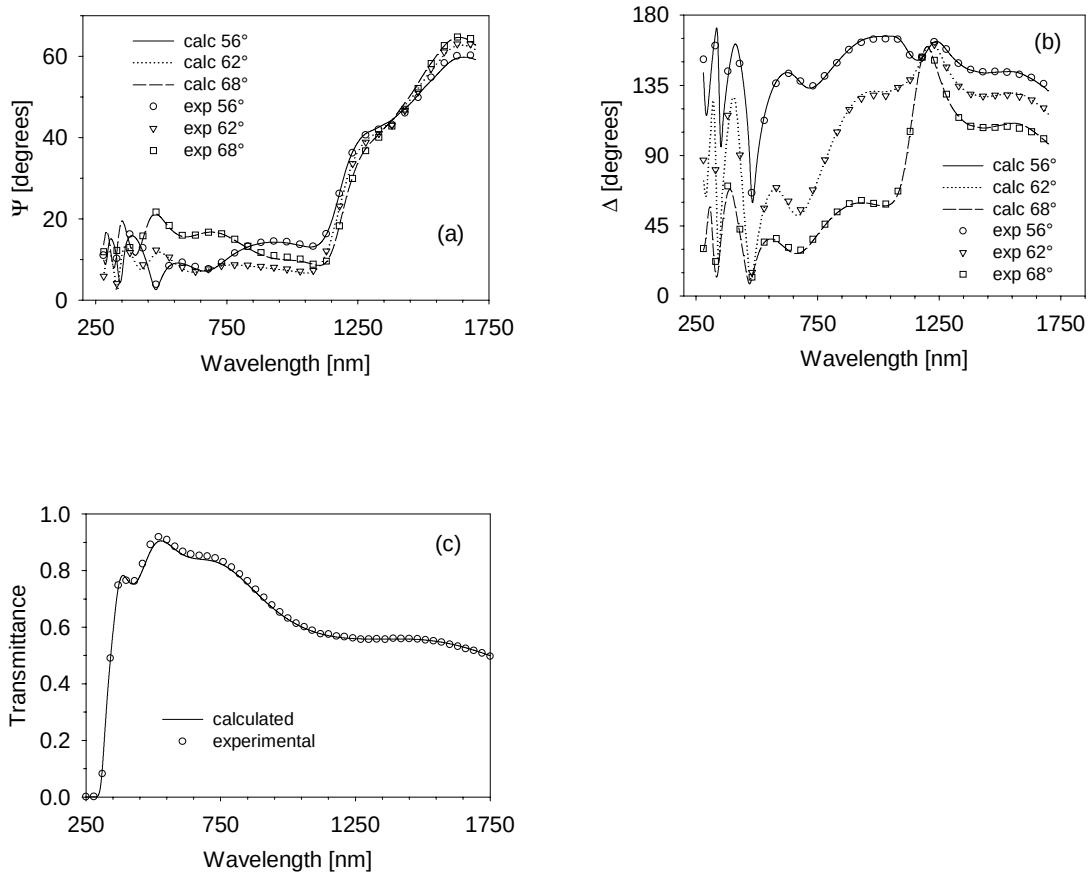

Figure 6. Experimental and calculated data on ellipsometric Ψ (part a) and Δ (part b), as well as spectrophotometric transmittance (part c), for Sn oxide film sputter deposited at an oxygen partial pressure of 4.5 mTorr. Different symbols and curves refer to data for the three indicated angles (in degrees).

IV. OPTICAL PROPERTIES: DATA AS A FUNCTION OF DEPOSITION PARAMETERS AND POSTTREATMENT

The optical properties, specifically the complex refractive index $N = n + ik$, depend on the deposition parameters. The optical constants, n and k, are referred to as refractive index and extinction coefficient, respectively. Figure 7 shows n at $\lambda = 550$ nm as a function of $p(O_2)$ for Sn oxide films. It appears that n has a minimum close to the flow ratio where the transition to a conductive SnO_2-like material takes place (cf. Fig. 2).

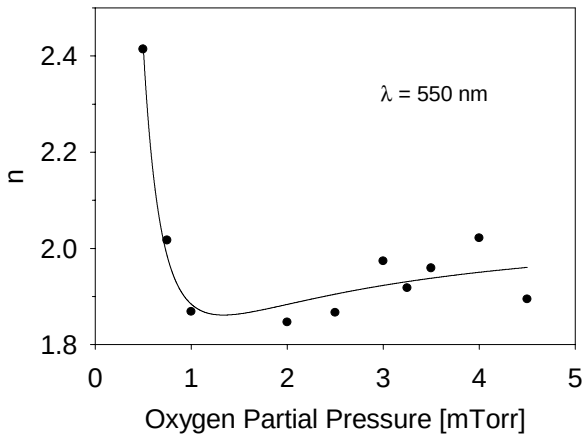

Figure 7. Refractive index vs. oxygen partial pressure for sputter deposited Sn oxide thin films. Data were taken at the shown wavelength λ. Symbols denote experimental data and and curves were drawn for convenience.

Figure 8a and b show the optical constants at low oxygen flow rates in the energy range 4.15 to 0.5 eV, corresponding to $300 < \lambda < 2500$ nm. The peak associated with the maximum in n undergoes a red shift and broadens with decreasing oxygen flow rate. The effect on the transmittance can be seen in Fig. 8c. Decreasing $p(O_2)$ from 2 to 0.5 mTorr causes the transition from transparent SnO_2 to brownish SnO [13]. Above $p(O_2) = 2$ mTorr, the transmittance remains essentially independent of oxygen content in the full spectral range.

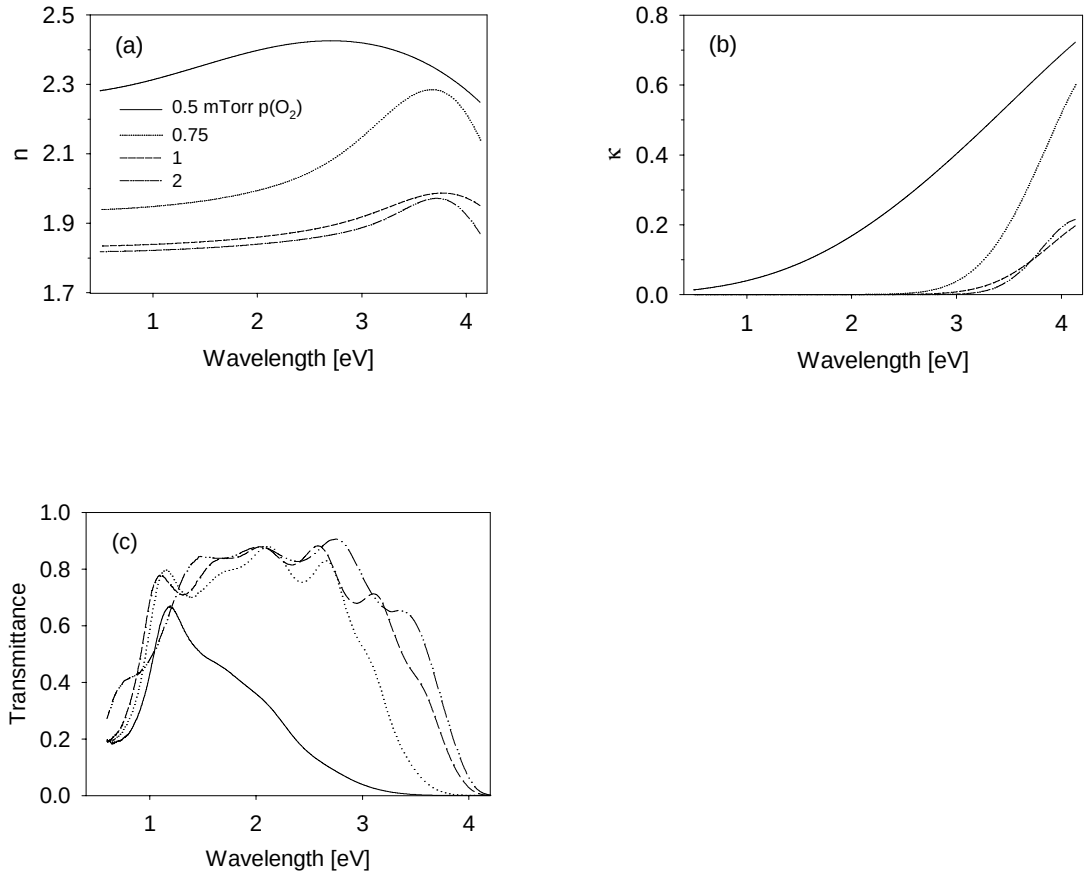

Figure 8. Spectral refractive index (part a), extinction coefficient (part b), and transmittance (part c) of Sn oxide films sputter deposited at four magnitudes of the oxygen partial pressure, $p(O_2)$.

Sn-oxide-based films were also deposited with hydrogen gas flowing during the sputtering process. The motivations for such films are twofold: First, it is a way to introduce protons into the lattice already during the film-making process, which is of interest for solid state ionic devices operating with protonic conduction [33]. Second, the introduction of hydrogen into the Sn oxide lattice may change the structure and electronic properties in ways similar to those caused by the addition of dopants such as fluorine or antimony.

Figure 9a shows that the refractive index decreases monotonically with the addition of hydrogen gas to a sputter atmosphere with $p(O_2)$=4.5 mTorr. Changes in

the extinction coefficient (Fig. 9 b) and transmittance (Fig. 9 c) are less significant. RBS showed that the densities of films deposited at different hydrogen flow rates were comparable, and hence the addition of hydrogen does not seem to lead to a more open film structure, a fact that would otherwise explain the lowering of the refractive index.

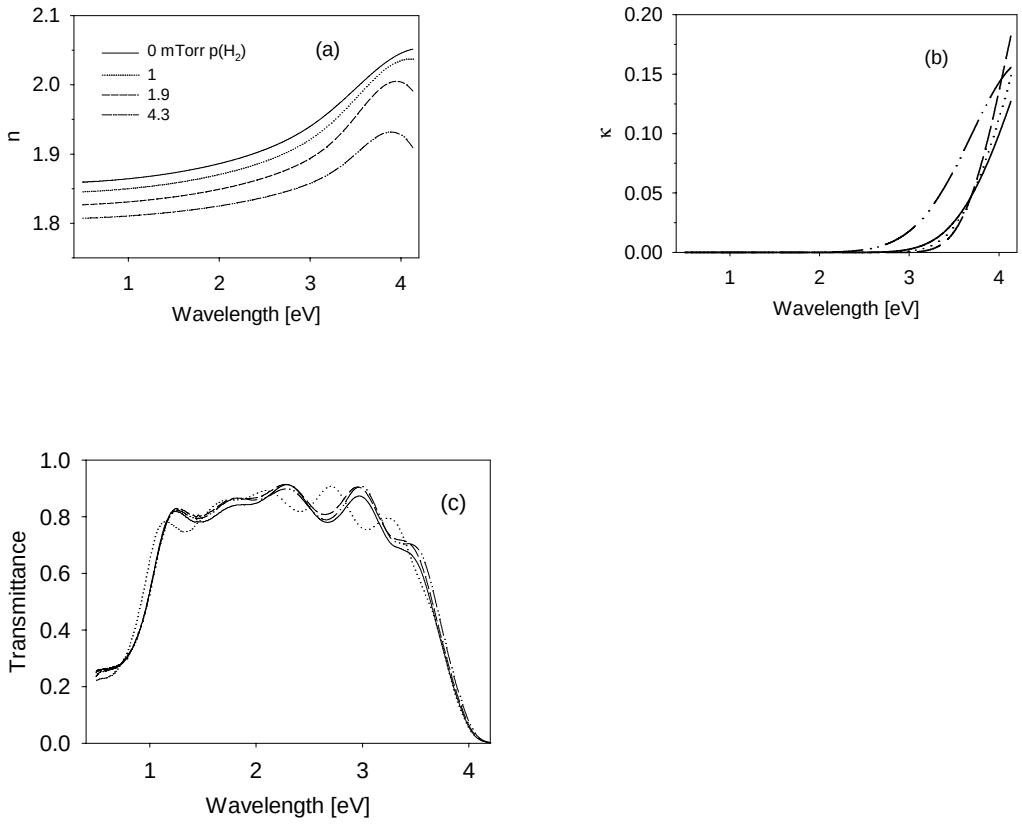

Figure 9. Spectral refractive index (part a), extinction coefficient (part b), and transmittance (part c) of sputtered deposited Sn-oxide-based films at four magnitudes of the hydrogen partial pressure, $p(H_2)$.

We evaluated the optical band gap energy E_g and showed that this parameter increased significantly in films produced in the presence of hydrogen. The evaluation was made by fitting the absorption coefficient α, defined by

$$\alpha = \frac{2\pi k}{\lambda}, \tag{3}$$

to the relation [34]

$$(E - E_g) \propto \sqrt{E \cdot \alpha}\,, \tag{4}$$

where E is the energy. Relation (4) presumes indirect optical transitions across the band gap. Figure 10 shows quantitative values of the band gap widening, which is as large as 0.13 eV for $p(H_2) \geq 2$ mTorr. The co-variation of refraction index and optical band gap is a manifestation of the well-known "Moss rule" [35] stating that

$$n^4 E_g = \text{constant}. \tag{5}$$

In the present case, the constant was 37 ± 1.

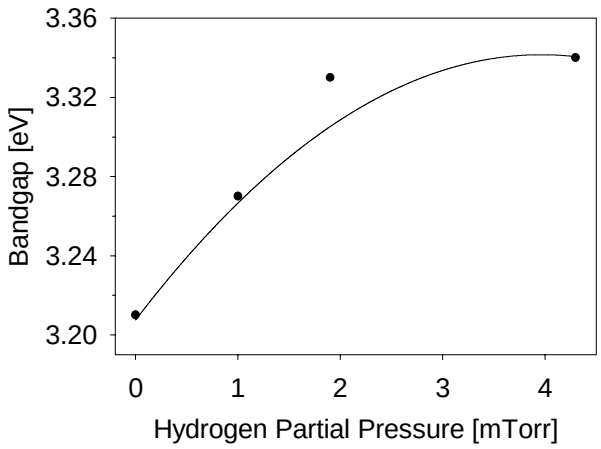

Figure 10. Optical band gap vs. hydrogen partial pressure for sputtered deposited Sn-oxide-based films. Symbols denote experimental data and the curve was drawn for convenience.

Electrochemical charge insertion/extraction showed that Sn oxide is an electrochromic material. Specifically, it is slightly cathodically coloring in the visible upon lithium insertion, as seen from Fig. 11c. The level of inserted Li^+ charge is indicated as the electrochemical potential versus lithium, as discussed in Sec. II. The refractive index is reported in Fig. 11a; it increases in the visible and near infrared as a function of the amount of charge insertion, and it decreases in the blue and ultraviolet

parts of the spectrum when the potentials are 2.0 and 1.7 V. This peculiar shift is seen in the extinction coefficient as well (Fig. 11b).

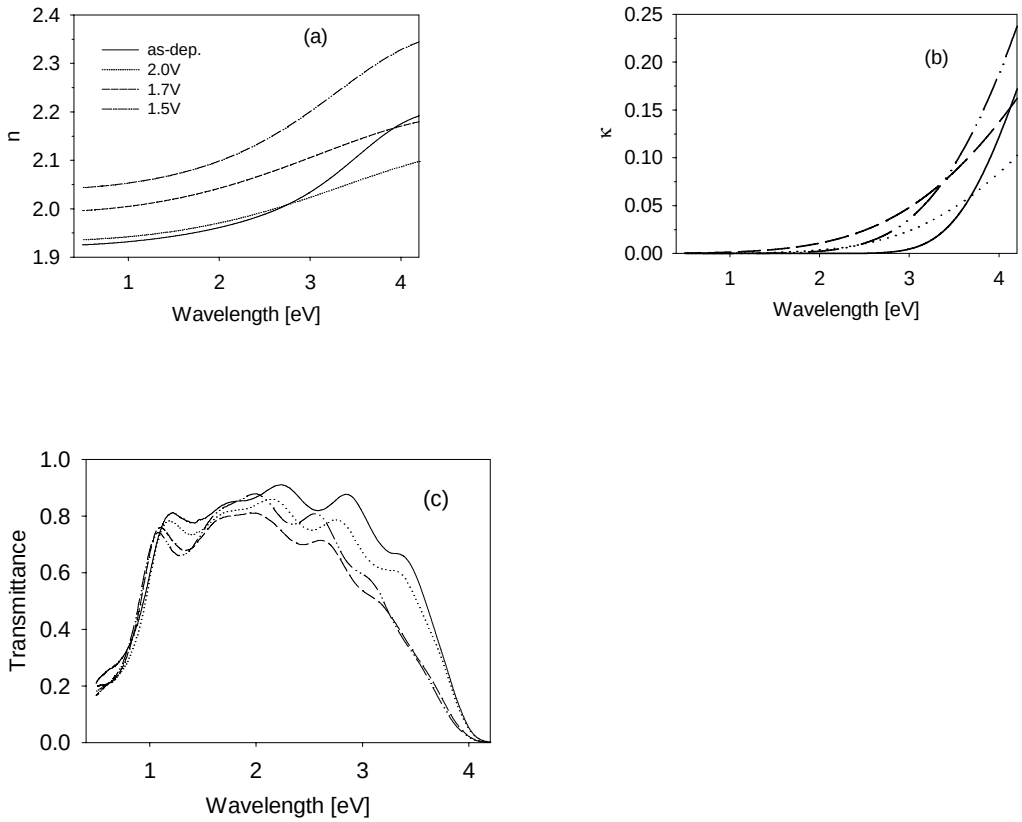

Figure 11. Spectral refractive index (part a), extinction coefficient (part b), and transmittance (part c) of a Sn-oxide-based film sputter deposited at an oxygen partial pressure of 4.5 mTorr. Data pertain to the as-deposited state and after electrochemical intercalation with lithium at three different voltages vs. Li/Li^+.

The ellipsometric analysis of the lithiated films showed that the thickness gradient of *n* was enhanced by the insertion of Li^+ in the Sn oxide, thereby indicating a non-homogenous distribution of lithium in the layer. Evidence for such a distribution was also found by NRA, as reported in Fig. 5 above. Figure 12 shows the refractive index at a wavelength of 550 nm as a function of the distance from the film surface.

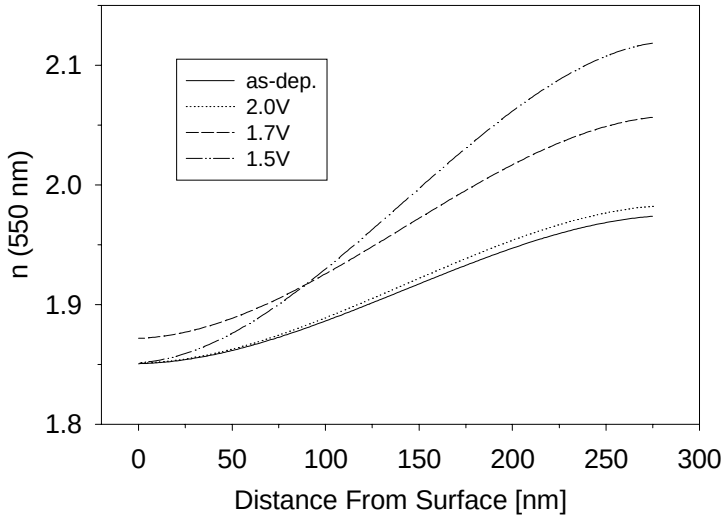

Figure 12. Refractive index vs. distance from the surface of a Sn-oxide-based film sputter deposited at an oxygen partial pressure of 4.5 mTorr. Data were taken at the shown λ. They pertain to the as-deposited state and after electrochemical intercalation with lithium at tree different voltages vs. Li/Li^+. The actual data correspond to "ladders" with five steps; smooth curves were drawn without loss of essential information in order to clearly display the refractive index profiles.

Whereas the *n* remains almost constant close to the surface, it rises significantly at the approach of the ITO layer. One may be tempted to assume an accumulation of lithium ions near to the ITO interface. However, the investigation by nuclear reaction analysis did not confirm this assumption, but instead showed slightly lower lithium content close to the ITO (cf. Fig 5). Obviously the refractive index gradient, as extracted from the model calculation, does not reflect the lithium distribution inside the film. It may be possible that the stress exerted on the Sn oxide film upon lithium insertion is larger close to where the film adheres to the substrate, thus there inducing a more significant change in the refractive index than near to the film surface, but nothing can be stated with certainty.

V. DISCUSSION AND CONCLUDING REMARKS

Optical constants of sputter deposited Sn oxide films were extracted from measurements on a structure that includes an ITO conductor by combining spectroscopic variable-angle ellipsometry with spectrophotometric measurements. The thickness of a surface roughness layer was obtained from optical data assuming a homogenous Sn oxide film with roughness. These data were compared with AFM measurements. These two methods gave consistent, though not quantitatively identical, results. By invoking a refractive index gradient across the Sn oxide film, the fit between theory and experiment was significantly improved thus indicating a less compact structure at the film surface. The addition of hydrogen gas during the sputtering process lowered the refractive index of the films; this effect is associated with a blue shift of the optical band gap. Our sample configuration allowed the Sn oxide films to be electrochemically reduced with lithium, so that a full set of properties could be determined for several charge states. Upon lithium insertion, the Sn-oxide-based films showed a weak cathodic electrochromism. Intercalation of charge raised the refractive index of the film and appeared to enhance the refractive index gradient across the film thickness.

ACKNOWLEDGMENT

We gratefully acknowledge T. Richardson's help with the electrochemical tests and K.M. Yu's help with RBS and NRA measurements. Work in Sweden was carried out under the auspices of the Ångström Solar Center, financed by the Foundation for Strategic Environmental Research and by NUTEK. Work in the US was supported by the Assistant Secretary for Energy Efficiency and Renewable Energy, Office of

Building Technologies, Building Systems and Materials Division of the US Department of Energy under Contract No. DE-AC03-76SF00098.

REFERENCES

1 B. Stjerna, E. Olsson and C.G. Granqvist, “Optical and Electrical Properties of RF Sputtered Tin Oxide Films Doped with Oxygen Vacancies, F, Sb, or Mo”, J. Appl. Phys. **76**, 3797-3844 (1994)

2 I. Hamberg, J.S.E.M. Svensson, T.S. Eriksson, C.G. Granqvist, P. Arrenius and F. Norin, “Radiative Cooling and Frost Formation on Surfaces with Different Thermal Emittance: Theoretical Analysis and Practical Experience”, Appl. Opt. **26**, 2131-2136 (1987)

3 C.G. Granqvist, *Handbook of Inorganic Electrochromic Oxides* (Elsevier, Amsterdam, 1995)

4 V. Lantto, “Semiconductor gas sensors based on SnO_2 thick films”, in *Gas Sensors*, edited by G. Sberveglieri, pp. 117-167 (Kluwer, Dordrecht, 1992)

5 W. Göpel and K.D. Schierbaum, "SnO_2 Sensors: Current Status and Future Prospects", Sensors and Actuators B **26-27**, 1-12 (1995)

6 T. Brousse, R. Retoux, U. Herterich and D.M. Schleich, “Thin-Film Crystalline SnO_2-Lithium Electrodes”, J. Electrochem. Soc. **145**, 1-4 (1998)

7 I.A. Courtney and J.R. Dahn, “Electrochemical and In-Situ X-Ray Diffraction Studies of the Reaction of Lithium with Tin Oxide Composites”, J. Electrochem. Soc. **144**, 2045-2052 (1997)

8 Y. Idota, T. Kubota, A. Matsufuji, Y. Maekawa and T. Miyasaka “Tin-Based Amorphous Oxide: A High-Capacity Lithium-Ion-Storage Material”, Science **276**, 1395-1397 (1997)

9 P. Olivi, E.C. Pereira, E. Longo, J.A. Varella and L.O. de S. Bulhoes, “Preparation and Caracterization of a Dip-coated SnO_2 Film for Transparent Electrodes for Transmissive Electrochromic Devices”, J. Electrochem. Soc. **140**, L81-L82 (1993)

10 B. Orel, U. Lavrencic-Stangar and K. Kalcher, “Electrochemical and Structural Properties of SnO_2 and Sb:SnO_2 Transparent Electrodes with Mixed Electronically Conductive and Ion-Storage Characteristics”, J. Electrochem. Soc. **141**, L127-L130 (1994)

11 U. Opara Krasovec, B. Orel, S. Hocevar and I. Musevic, “Electrochemical and Spectroelectrochemical Properties of SnO_2 and SnO_2/Mo Transparent Electrodes with High Ion Storage Capacity”, J. Electrochem. Soc. **144**, 3398-3409 (1997)

12 J. Isidorsson and C.G. Granqvist, “Electrochromism of Li-intercalated Sn Oxide Films made by Sputtering”, Solar Energy Mater. Solar Cells **44**, 375-381 (1996)

13 J. Isidorsson, C.G. Granqvist, L. Häggström and E. Nordström, “Electrochromism in Lithiated Sn Oxide: Mössbauer Spectroscopy Data on Valence State Changes” J. Appl. Phys. **80**, 2367-2371 (1996)

14 K. von Rottkay and M. Rubin, "Optical Indices of Pyrolitic Tin-Oxide Glass", in *Polycrystalline Thin Films: Structure, Texture, Properties and Applications II*, H.J. Frost, M.A. Parker, C.A. Ross and E.A. Holm, eds, Mater. Res. Soc. Symp. Proc. **426**, pp. 449-454 (1996)

15 F.K. Urban III, P. Ruthakowski Athey and M.D. Islam, "Modeling of Surface Roughness in Variable-Angle Spectroscopic Ellipsometry using Numerical Processing of Atomic Force Microscopy Images", Thin Solid Films **253**, 326-332 (1994)

16 P. Ruzakowski Athey, F.K. Urban III and P.H. Holloway, "Use of Multiple Analytical Techniques to Confirm Improved Optical Modelling of SnO_2:F Films by Atomic Force Microscopy and Spectroscopic Ellipsometry", J. Vac. Sci. Technol. B **14**, 3436-3444 (1996)

17 A. Roos, “Optical Properties of Pyrolytic Tin Oxide on Aluminum”, Thin Solid Films **203**, 41-48 (1991)

18 F. Caccavale, R. Coppola, A. Menelle, M. Montecchi, P. Polato and G. Principi, "Characterization of SnO_x on Architectural Glass by Neutron Reflectometry, SIMS, CEMS and Spectrophotometry", J. Non-Cryst. Solids **218**, 291-295 (1997)

19 R.J. Martin-Palma and J.M. Martinez-Duart, "Accurate Determination of the Optical Constants of Sputter-Deposited Ag and SnO_2 for Low Emissivity Coatings", J. Vac. Sci. Technol. **A 16**, 409-412 (1998)

20 G. Lévêque and Y. Villachon-Renard, "Determination of Optical Constants of Thin Film From Reflectance Spectra", Appl. Opt. **29**, 3207-3212 (1990)

21 C. Herzinger and B. Johs, "The Parametric Semiconductor Model", in *Guide to Using WVASE32* , pp. 347-349 (J.A. Woollam Co., Lincoln, NE, 1996)

22 C.C. Kim, J.W. Garland, H. Abad and P.M. Raccah, "Modeling the Optical Dielectric Function of Semiconductors: Extension of the Critical-Point Parabolic-Band Approximation", Phys. Rev. B **45**, 11749-11767 (1992)

23 X.-F. He, "Interband Critical-Band Line Shapes in Confined Semiconductor Structures with Arbitrary Dimensionality: Inhomogeneous Broadening" J. Opt. Soc. Am. B **14**, 17-20 (1997)

24 W.H. Preuss, B.P. Flannery, S.A. Teukolsky and W.T. Vetterling, *Numerical Recipes*, pp. 523-528 (Cambridge University Press, Cambridge, 1989)

25 I. Hamberg and C.G. Granqvist, "Evaporated Sn-Doped In_2O_3 Films: Basic Optical Properties and Applications to Energy-Efficient Windows", J. Appl. Phys. **60**, R123-R160 (1986)

26 K. von Rottkay, M. Rubin and N. Ozer, "Optical Indices of Tin-Doped Indium Oxide and Tungsten Oxide Electrochromic Coatings", in *Thin Films for Photovoltaic and Related Device Applications*, D. Ginley, A. Catalano, H. W. Schock, C. Eberspacher, T. M. Peterson and T. Wada, eds, Mater. Res. Soc. Symp. Proc. **403**, pp. 551-556 (1996)

27 J. Szczyrbowski, K. Schmalzbauer and H. Hoffman, "Optical Properties of Rough Thin Films", Thin Solid Films **130**, 57-73 (1985)

28 D.E. Aspnes and J.B. Theeten, "Investigation of Effective-Medium Models of Microscopic Surface Roughness by Spectroscopic Ellipsometry", Phys. Rev. B **20**, 3292-3302 (1979)

29 C. Pickering, R. Greef and A.M. Hodge, “Characterisation of Rough Silicon Surfaces using Spectroscopic Ellipsometry, Reflectance, Scanning Electron Microscopy and Scattering Measurements”, Mater. Sci. Eng. B **5**, 295-299 (1990)

30 D. Rönnow, S.K. Andersson and G.A. Niklasson, “Surface Roughness Effects in Ellipsometry: Comparition of Truncated Sphere and Effective Medium Models”, Opt. Mater. **4**, 815-821 (1995)

31 D.E. Aspnes, "Microstructural Information From Optical Properties in Semiconductor Technology", in *Optical Characterization Techniques for Semiconductor Technology*, D.E. Aspnes, S. So and R.F. Potter, eds., Proc. Soc. Photo-Opt. Instrum. Eng. Vol. **276**, 188-195 (1981)

32 D.A.G. Bruggeman, "Berechnung verschiedener physikalischer Konstanten von heterogenen Substanzen", Ann. Phys. (Leipzig) **24**, 636-664 (1935)

33 A. Azens, L. Kullman, G. Vaivars, H. Nordborg and C.G. Granqvist, Solid State Ionics, to be published

34 F. Wooten, *Optical Properties of Solids* (Academic, New York, 1981)

35 T.S. Moss, *Optical Properties of Semiconductors* (Butterworth, London, 1959)